INTERNATIONAL JOURNAL FOR NUMERICAL AND ANALYTICAL METHODS IN GEOMECHANICS
Int. J. Numer. Anal. Meth. Geomech. 2013; **37**:1987–2004
Published online 1 August 2012 in Wiley Online Library (wileyonlinelibrary.com). DOI: 10.1002/nag.2116

Stability of earth slopes. Part II: three dimensional analysis in closed-form

Lysandros Pantelidis[1,*,†] and D.V. Griffiths[2,3]

[1]*Department of Civil Engineering and Geomatics, Cyprus University of Technology, 3603 Lemesos, Cyprus*
[2]*Department of Civil and Environmental Engineering, Colorado School of Mines, Golden, CO 80401, United States*
[3]*Australian Research Council Centre of Excellence for Geotechnical Science and Engineering, University of Newcastle, Callaghan NSW 2308, Australia*

SUMMARY

A closed-form stability analysis of earth slopes performed in 3D is proposed. The sliding surface is assumed spherical and treated as a rigid body allowing the internal state of stress to be ignored. The proposed closed-formed solution (CFS) can be applied to both homogenous and non-homogenous slopes of either simple or complex geometry and can also deal with any kind of additional loading. Although it is recognized that the critical failure surface is often non-spherical, the CFS methodology for spheres described herein provides an objective tool for the evaluation of the assumptions made by other limit equilibrium methods including the role of intercolumn forces. Copyright © 2012 John Wiley & Sons, Ltd.

Received 11 May 2011; Revised 29 February 2012; Accepted 23 May 2012

KEY WORDS: slope stability; closed-form solution; lumped mass approach; 3D analysis; rigid body rotation

1. INTRODUCTION

Based on published works, it can be said that the decade of the 1960s was the most productive as regards development of methods for the stability analysis of slopes in two dimensions. In the next decade, interest in inventing new 2D methods or refining existing ones declined with a simultaneous increase in interest in methods of stability analysis of slopes in 3D. Indeed from the mid 1970s until today, a large number of 3D limit equilibrium methods have been proposed (e.g. [1–3] and [4]). This growth of interest in 3D slope stability analysis is related to the falling costs and increased computational power available through personal computers.

As regards limit equilibrium methods, in most cases, slices in 2D have been replaced by columns in 3D, which means that not only does the problem remain statically indeterminate, but additional assumptions are needed regarding the third dimension. Although this paper focuses on 3D limit equilibrium methods, it is recognized that other approaches are available for 3D slopes, including extrapolation of 2D slope stability to 3D (e.g. [5]), limit analysis methods (e.g. [2, 6–9] and [10]), and non-linear finite element methods (e.g. [11, 12] and [13]). Detailed reviews of existing limit equilibrium methods performed in three dimensions have already been reported in numerous papers and textbooks (e.g. [14, 15] and [16]), hence they will not be repeated here.

The proposed closed-form solution that follows is the 3D counterpart of the method presented in the companion paper of Part I. Therefore, similar to the previous work, the whole slope mass over the slip surface, which is considered spherical, is idealized as a single point, the center of mass (Figure 1). This is feasible because spherical failure is displaced as a rigid body rotation; therefore, no assumptions are

*Correspondence to: Lysandros Pantelidis, Department of Civil Engineering and Geomatics, Cyprus University of Technology, P.O. Box 50329, 3603 Lemesos, Cyprus.
†E-mail: lysandros.pantelidis@cut.ac.cy

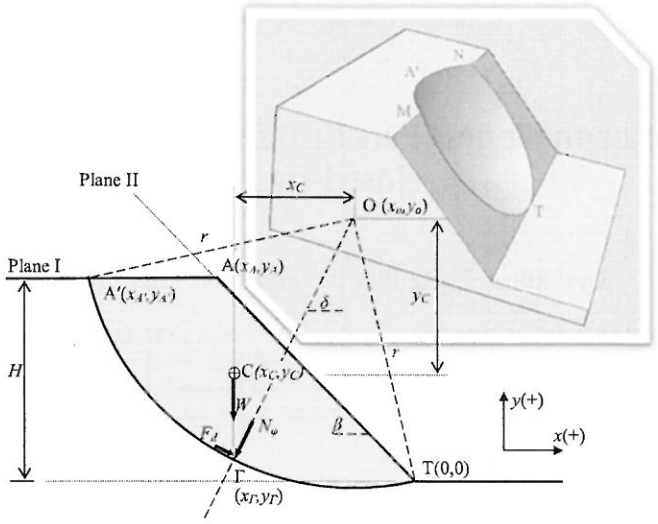

Figure 1. Example of a simple homogenous slope. The whole failure mass (gray area) is idealized as a single point (point C; center of mass). Projection of weight W to the slip surface (point Γ).

necessary regarding the internal state stress within the soil mass. This is in contrast to non-spherical failure surfaces, which can induce internal stresses within the sliding volume.

2. SCOPE OF THE PAPER

The authors recognize that the actual failure surface of slopes is not necessarily spherical. However, the proposed 3D closed-form solution can be used as benchmark for the evaluation of existing 3D slope stability methods and their assumptions. Moreover, it could be used as an objective tool for the interpretation of the internal forces if, at a later stage, the sliding mass is divided into columns. The interpretation of the internal state of stress of the sliding mass involves the determination of the point and angle of action of intercolumn forces based on a parametric analysis of the factors that may influence these magnitudes (e.g. shear strength characteristics of soils, gradient of column base or top). Such a study may lead to the proposal of a new, more effective, 3D limit equilibrium method for the stability of earth slopes applicable to any failure surface shape. The proposal of a new 3D slope stability method based on the concept of columns as well as the study of intercolumn forces are beyond the scope of the present paper.

3. DEFINITION OF SAFETY FACTOR

The factor of safety for slope stability analysis is usually defined as the ratio of the ultimate shear strength divided by the mobilized shear stress at working stress levels. Although there are several ways of formulating the factor of safety FS, for the special case of spherical failure studied herein, the expression of safety factor in terms of moments is the most appropriate:

$$FS_M = \frac{\text{Resisting moments}}{\text{Driving moments}} = \frac{M_f}{M_d} \tag{1}$$

where M_f is the sum of the resisting moments and M_d is the sum of the driving moments.

The center of the sphere is taken as the moment point for convenience. The factor of safety is assumed to be the same at all points along the slip surface, which is typical for the conventional limit equilibrium methods (e.g. [15]). As shown below, the proposed methodology satisfies force equilibrium as well.

DOI: 10.1002/nag

4. BACKGROUND TO THE PROPOSED METHOD

The methodology presented herein is based on the fact that, at the initiation of pure rotational slides along a spherical surface, no shear forces are developed inside the failure mass. This allows for the internal forces to be ignored and the mass over the slip surface to be idealized as a single point, the center of (failure) mass (Figure 1). Similarly, other possible forces acting on the slope (e.g. pore pressures, seismic, footing, water in tension crack etc) can be projected onto the failure surface before calculating their moment about the center of rotation.

Adopting Coulomb's equation and working in effective stresses (Equation 2) with the homogenous slope in which only gravity and pore pressures act, the safety factor, FS_{3d}, is given by Equation (3). The radius r in Equation (3) cancels out, thus, the proposed methodology satisfies force equilibrium as well. Detailed analysis of the forces included in the equation in question is given in the next section. Moreover, examples of some of the most commonly used forces in slope stability analysis are given in Section 6.

$$\tau_f = c' + (\sigma\text{-}u)\tan\varphi' = c' + \sigma\tan\varphi'\text{-}u\tan\varphi' \tag{2}$$

$$\begin{aligned} FS_{3d} &= \frac{c'A_{ss}r + W\cos\left(\frac{\pi}{2}\text{-}\delta\right)\tan\varphi' r\text{-}\sum u\tan\varphi' r}{W\sin\left(\frac{\pi}{2}\text{-}\delta\right)r} = \\ &= \frac{c'A_{ss} + W\cos\left(\frac{\pi}{2}\text{-}\delta\right)\tan\varphi'\text{-}U\tan\varphi'}{W\sin\left(\frac{\pi}{2}\text{-}\delta\right)} = FS_{3d,F} \end{aligned} \tag{3}$$

5. FORCES ACTING ON THE SLIP SURFACE

5.1. *Force* $\boldsymbol{F_c}$ because of cohesion

The resisting force because of cohesion is derived from the product of cohesion, c', by the area, A_{ss}, of slip surface:

$$F_c = c'A_{ss} \tag{4}$$

Unfortunately, there is not a formula currently available that can give directly the surface area of a sphere between two or more non-parallel planes that intersect the sphere; planes representing the slope face, the upslope area of the slope and in case of deep seated failures, the downslope area). However, the area in question can be calculated indirectly but without sacrificing accuracy following *Archimedes of Syracuse* (287–212 BC). The well-known formula for the surface area of sphere ($A_{sph}=4\pi r^2$) was first derived by Archimedes based upon the fact that the projection of a sphere onto a circumscribing cylinder is area preserving. The method is simple and has been widely used since 1772 in cartography (cylindrical equal-area projection).

The procedure for calculating the area of the required spherical surface is described below:

- *Definition of planes and intersection points*: The upslope area is represented by a plane passing through the points A and A′ (Plane I), whereas the slope face is represented by a plane passing through the points T and A (Plane II). Both planes are assumed to be parallel to the $z-$axis, although as shown later, this is not a restriction. Plane I, Plane II and the sphere have two points in common, namely, M and N; see Figure 1.
- *Area* A_{ss} *of slip surface*: The area in question arises indirectly from its radial projection to an imaginary cylinder that circumscribes the sphere; the axis of the cylinder is considered parallel to the $z-$axis (Figure 2). The projected area is equal to the original area on the sphere. The radial

DOI: 10.1002/nag

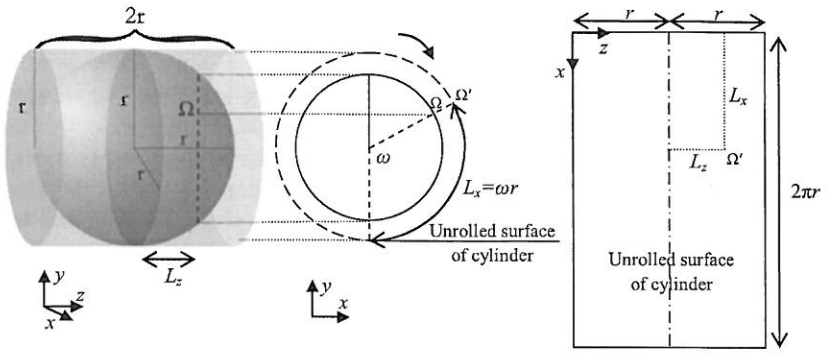

Figure 2. Sphere of diameter $D=2r$ with a circumscribing cylinder of height $H_{cyl}=2r$. Example: projection of point Ω onto a $z-x$ plane.

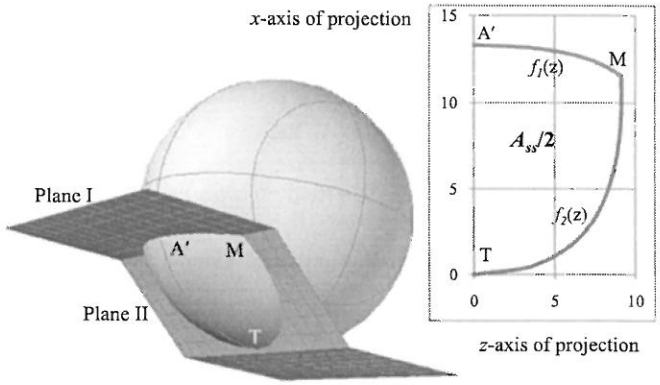

Figure 3. *3D drawing*: Internal view of failure surface. *Projection diagram*: projection of failure surface onto a $z-x$ plane (semi-diagram, symmetry as for the x-axis).

projection is done in a vertical[1] manner, whereas as the diameter of the sphere is equal to the height of the cylinder, all points preserve their original z −coordinate. The cylinder is then 'unrolled' and the result is a $z-x$ diagram similar to the example given in Figure 3. In essence, only the points of intersection between the slip surface and the slope profile are projected. These points can easily be represented by mathematical (e.g. polynomial) functions. The area A_{ss}, finally, derives from the subtraction of the integrals of the upper and lower function (Figure 3, Equation 5). The authors propose in the Appendix an analytical formula for the exact calculation of the area in question. The formula stands for symmetrical failures as for the x-y plane ($z=0$) passing through the toe of the slope whilst, moreover, as regards to the geometry of the problem it stands that, the upslope area is horizontal, the point of origin is the toe of slope for $z=0$, the slope face is represented by a plane parallel to the z-axis and the slope is above the negative part of x-axis (see Figure 1). For other cases the formula must be modified as needed.

$$A_{ss} = 2\int \{f_1(z) - f_2(z)\}dz \tag{5}$$

Heterogeneity: If the slip surface meets soil layers with different cohesions (Figure 4), Eq. (4) is modified accordingly, and the procedure is analogous to the one presented above; division of slip surface into parts and direct projection of each one of them to the circumscribing cylinder is necessary.

[1]For better interpretation, readers may imagine a lamp moving along a horizontal axis that passes through the center of the sphere; this is also the axis of the circumscribing cylinder. The beam produced by the lamp shines only perpendicularly to the z-axis, around of which, the lamp is free to rotate. The shade of every surface point of sphere onto the cylinder is a projected point.

DOI: 10.1002/nag

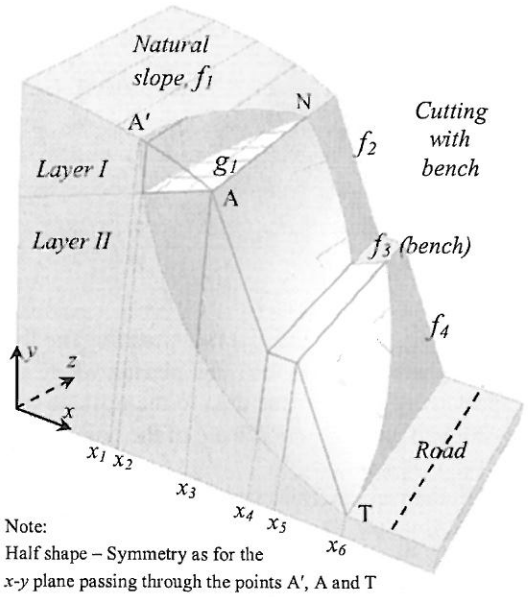

Figure 4. Example of a heterogeneous slope with complex geometry. The sliding mass is divided by the interlayer plane (g_1)and vertical planes passing through points x_1 to x_6 into six (homogenous) parts, whereas the free ground surface consists of four parts (functions f_1 to f_4). The failure surface crosses two soil layers.

Upslope area: The upslope area can be any plane (horizontal or inclined) or even a curved surface. This area is represented by mathematical function(s), and the intersection points with the sphere are determined.

5.2. *Friction and driving force,* $\boldsymbol{F_\varphi}$ and $\boldsymbol{F_d}$, respectively

In this case, the weight, W, of the whole failure mass, as well as, the $x-$coordinate of its center of mass, x_C, must be known. The weight in question corresponds to the volume of the slope mass enclosed between the failure surface and the free ground surface (Figure 1, gray area). The method can be used in homogenous and non-homogenous slopes and in either simple or complex geometries (see Figures 1 and 4) following the steps below:

i. The free ground surface is divided into n parts, such that each one of them can be represented by a (simple) function $y=f_i(x)$, $i=1,2,\ldots n$ ($y=f_i(x,z)$ if the plane is not parallel to the $z-$axis).
ii. If there are $m+1$ soil layers of different unit weights and shear strength characteristics, each layer is separated by a line represented by a function (or a number of successive functions) $y=g_i(x)$, $i=1,2,\ldots m$($y=g_i(x,z)$ if the plane is not parallel to the $z-$axis).
iii. The failure mass is then divided into q parts, each one of them homogenous encompassed by an upper and a lower function ($f_i(x)$ and $g_i(x)$ or $f_i(x)$ and $f_{sph}(x)$ or $g_i(x)$ and $f_{sph}(x)$) and two x values as boundaries and finally,
iv. The gravity force, W, and the $x-$coordinate of the center of the mass, x_C, are given by Equations (6a) and (7), respectively. The equations shown below refer to the specific homogenous slope shown in Figure 1. For other cases, they should be modified as needed.

$$W = W_1 + W_2 \tag{6a}$$

$$W_1 = \int_{x_{A'}}^{x_A} \int_{-\sqrt{r^2-\{f_{AA'}(x)-y_o\}^2-(x-x_o)^2}}^{\sqrt{r^2-\{f_{AA'}(x)-y_o\}^2-(x-x_o)^2}} \gamma_s \left[f_{AA'}(x)-f_{sph}(x,z)\right] dzdx = \\ = \iint f_{W1}(z,x)dzdx \tag{6b}$$

DOI: 10.1002/nag

$$W_2 = \int_{x_A}^{x_T} \int_{-\sqrt{r^2-\{f_{AT}(x)-y_o\}^2-(x-x_o)^2}}^{\sqrt{r^2-\{f_{AT}(x)-y_o\}^2-(x-x_o)^2}} \gamma_s \left[f_{AT}(x)-f_{sph}(x,z) \right] dzdx = \\ = \iint f_{W2}(z,x)dzdx \tag{6c}$$

$$x_C = \frac{\text{total moments}}{\text{total weight}} = \frac{\iint x f_{W1}(z,x)dzdx + \iint x f_{W2}(z,x)dzdx}{W} \tag{7}$$

where for the slope of Figure 1 is $f_{AA'}(x) = H$ and $f_{AT}(x) = -\tan\beta x$. The limits of the internal integrals derive from the equation of the sphere solved as for z and placing where y the equation that represents the slope profile, in this respect $y = f_{AA'}(x)$ for the area to the upslope of the slope and for the slope face. In essence, these limits correspond to z −coordinate of the points of intersection between the slip surface and the slope profile for $x_A \le x \le x_{A'}$.

The procedure continues with the vertical projection of the force W onto the failure surface, where it is broken into tangential (F_d) normal (N_φ) components. The first one is the driving force because of gravity (see Equation 3), whereas the second one is multiplied by the friction coefficient,$\tan\varphi'$, to give the total friction force $F_\varphi$that corresponds to the product $\sigma\tan\varphi'$from Eq. (2), hence:

$$F_d = W\sin(^{\pi}/_{2}-\delta) \tag{8}$$

$$F_\varphi = N_\varphi \tan\varphi' = W\cos(^{\pi}/_{2}-\delta)\tan\varphi' \tag{9}$$

where from Figure 1(a), $\delta = \tan^{-1}(y_T/x_T)$.

The above procedure involves a major assumption regarding the point of action of F_d and N_φ,which is considered to be the point of action of W on the slip surface. Following a procedure similar to the one given in the Appendix of Part I, it can be shown that the assumption made herein is also not true. As in the 2D case, the resultant normal and driving force, as well as the point of action of these forces can be obtained by integrating along the spherical slip surface. The procedure in question which requires division of the sliding mass into columns, is presented in the Appendix at the end of the paper. Generally, it can be said that both the rigorous approach presented in the Appendix and the simplified one result to the same safety factor values. Thus, the two components of W on the slip surface (F_d and N_φ) can be considered representative of the resultant normal and driving force of the failure mass.

Heterogeneity: If the slip circle meets k soil layers with different friction angles φ'_k, then k driving and friction forces must be calculated. Each pair of forces corresponds to the mass above the part/area of the slip surface that has the same φ'. For example, in the two-layer system of Figure 4, one pair of forces should be calculated for x_1 to x_2 and one for the rest going from x_2 to x_6.

It is apparent that in case of heterogeneous slopes, the sliding mass is divided into parts (e.g. two parts for a two-layer system, three parts for a three-layer system, etc). Although, the present CFS ignores the inter-part forces, it is believed that as the number of interfaces created in the analysis is small, the error in the resulting safety factor value is minor. It may be noted that in the case of various methods of columns where the number of columns is very small, the main source of error is because of the fact that the failure surface is represented by a coarse polygonal surface, something that is avoided by the present method where the spherical surface is strictly retained. On the other hand, if the number of columns in a method of columns is great enough for the failure surface to be closely represented by a smooth polygonal surface, the error in the safety factor value is mainly because of the assumptions made for the intercolumn forces. Comparison studies have already shown that the different methods of columns give usually similar results (e.g. see [1, 17]).

DOI: 10.1002/nag

Center of mass: If the problem is not fully symmetrical (geometry and layering) as for the plane $x-y$, in addition to x_C (Equation 7), the z_C coordinate must be calculated whilst the angle δ must be modified accordingly.

Surfaces non-parallel to the z-axis: The proposed closed-form solution can also deal with surfaces not parallel to the $z-$axis (e.g. $f_i(x,z)$). In this case, Equations (6a)–(6c) should be modified accordingly, and because of the absence of symmetry, the z_C coordinate of the center of the mass must also be known for the calculation of the angle δ (see Equations 8 and 9). The angle δ refers to the acute angle between the vertical line passing through the center of the sphere and the line that connects the last with the point of projection of the center of the mass on the slip surface.

5.3. *Pore pressure force* F_w

The pore pressure distribution is shown in Figure 5 denoted as function $u(x,z)$. The resultant pore pressure force U can be calculated according to Equation (10), as the area bounded between this surface and the spherical failure surface. However, as γ_w is constant, it is more convenient for U to be calculated directly from the area between the free water surface and the slip surface, where all functions are already known according to Equations (11a)–(11c).

$$U=\int_{x_{B'}}^{x_T}\int_{-z(x)}^{z(x)}u(x,z)dzdx=\int_{x_{B'}}^{x_T}\int_{-z(x)}^{z(x)}\left\{\gamma_w f_{wt}(x)\text{-}\gamma_w f_{sph}(x,z)\right\}dzdx \tag{10}$$

where, $z(x)=\sqrt{r^2-\left\{f_{wt}(x)-y_o\right\}^2-(x-x_o)^2}$

$$U=U_1+U_2 \tag{11a}$$

$$U_1=\int_{x_{B'}}^{x_B}\int_{-\sqrt{r^2-\left\{f_{BB'}(x)-y_o\right\}^2-(x-x_o)^2}}^{\sqrt{r^2-\left\{f_{BB'}(x)-y_o\right\}^2-(x-x_o)^2}}\gamma_w\left\{f_{BB'}(x)\text{-}f_{sph}(x,z)\right\}dzdx=\iint f_{u1}(x,z)dzdx \tag{11b}$$

$$U_2=\int_{x_B}^{x_T}\int_{-\sqrt{r^2-\left\{f_{BT}(x)-y_o\right\}^2-(x-x_o)^2}}^{\sqrt{r^2-\left\{f_{BT}(x)-y_o\right\}^2-(x-x_o)^2}}\gamma_w\left\{f_{BT}(x)\text{-}f_{sph}(x,z)\right\}dzdx=\iint f_{u2}(x,z)dzdx \tag{11c}$$

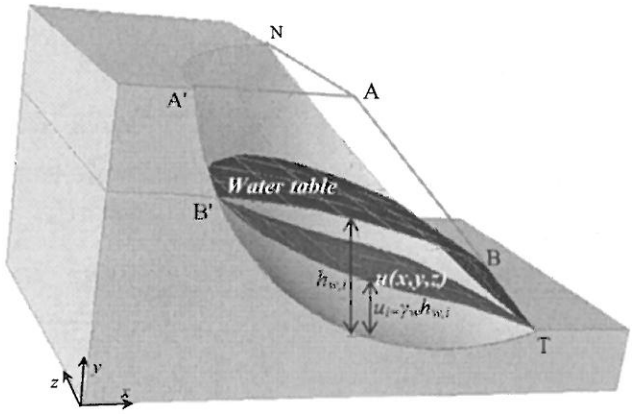

Figure 5. Example: water table in slope and pore pressure distribution along the failure surface (function $u(x,y,z)$).

DOI: 10.1002/nag

The buoyancy force U, which acts radially on the slip surface, is multiplied directly by the friction coefficient $\tan\varphi'$ giving the force F_u that corresponds to the negative term $u\tan\varphi'$ in Coulomb's equation (Equation 2), that is:

$$F_u = U\tan\varphi' \tag{12}$$

For information purposes, it is noted that U acts at the intersection point between the radius passing through the centroid C' of the area bounded between the free water surface and the slip surface. If the problem is fully symmetrical as for the $x-y$ plane it stands that $z_{C'} = 0$. Otherwise, the three coordinates are as follows:

$$x_{C'} = \frac{\iint x f_{u1}(x,z)dzdx + \iint x f_{u2}(x,z)dzdx}{U} \tag{13a}$$

$$y_{C'} = \frac{\iint y f_{u1}(y,z)dzdy + \iint y f_{u2}(y,z)dzdy}{U} \tag{13b}$$

$$z_{C'} = \frac{\iint z f_{u1}(z,x)dxdz + \iint z f_{u2}(z,x)dxdz}{U} \tag{13c}$$

6. EXTERNAL FORCES ACTING ON THE SLOPE

The methodology described is easily generalized to include other types of external forces commonly encountered in slope stability analysis. Some of these load cases are shown in Figure 6 and include water-filled tension cracks, pseudo-static earthquake loading (horizontal and vertical components), footing loading on the crest of the slope or elsewhere and pool loading because of free-standing water adjacent to the slope. As a general rule, additional forces of this type are projected onto the slip surface and broken into normal and tangential components. Each normal component is multiplied by both the coefficient of friction $\tan\varphi'$ and the slip circle radius r and then added to the numerator of the safety factor equation (Equation 3). The tangential component is multiplied only by the radius r before it is added to the denominator of the safety factor equation.

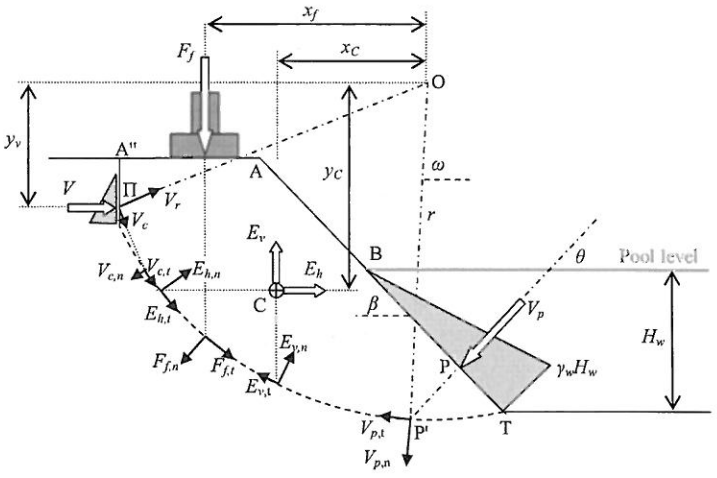

Figure 6. Example: possible external forces acting on a homogenous earth slope (see Figures 1 and 5 for more details about gravity force and pore pressures).

DOI: 10.1002/nag

Some additional comments are given below:

- *Heterogeneity*: If the slip circle meets various soil layers of different friction angle, φ', then the normal component of each weighing force W_i is multiplied by the respective coefficient of friction, tan φ_i'(Figure 7a). The same goes for the pore water pressures, where the distribution function $u(x, y, z)$ is divided in a manner similar to the one applied to W_i (division with vertical planes) with each part multiplied by the respective coefficient of friction.
- *Seismic force*: Pseudo-static seismic forces act at the center of the (sliding) mass and can be applied directly in homogenous earth slopes as shown in Figure 6. An additional step is needed if the slip surface crosses more than one layers (e.g. see Figure 8) in which case the failure mass should be divided into *horizontal* and/or *vertical* lines as needed, passing through the points on the slip surface where φ' changes. For every sub-area that arises from the division, both the magnitude of the earthquake forces and the coordinates of the centers of mass must be calculated. Following this, each gravity force is then multiplied by the required seismic coefficient. Finally, the forces are projected onto the slip surface and broken into normal and tangential component as described previously.
- *Pool loading*: This distribution is triangular following the pattern shown in Figures 6 and 9. Assuming that the problem is symmetrical, the resultant force V_p, which is given by Equation (14), acts perpendicular to the slope face at one third of the vertical height of the water (H_w) above the slope toe.

$$V_p = \frac{1}{2}\gamma_w H_w A_p \tag{14}$$

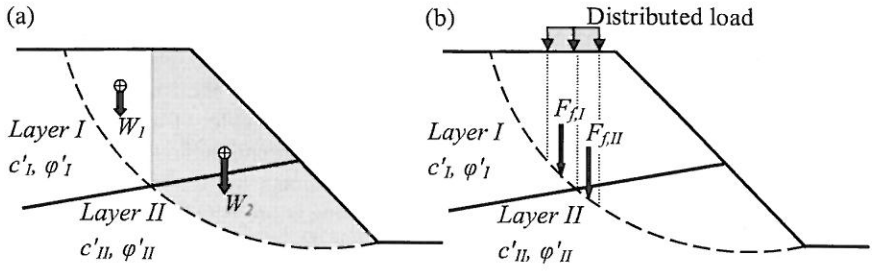

Figure 7. Non-homogeneous slopes: (a) vertical division of sliding mass and (b) division of a distributed load for changing φ' values on the slip surface.

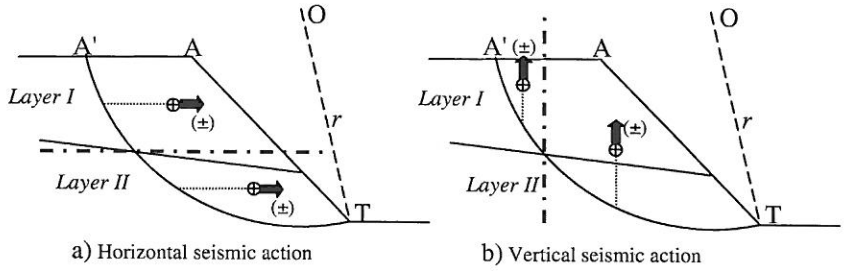

Figure 8. Horizontal and vertical seismic forces in two-layer slope system.

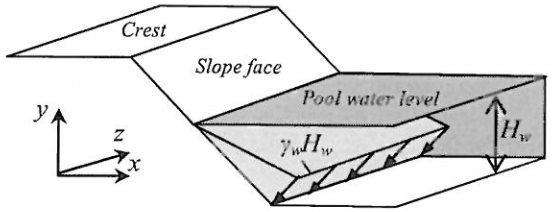

Figure 9. Pool loading: triangular distribution of water pressure on the slope face along the z-axis.

DOI: 10.1002/nag

The contact area A_p between the water and the slope face inside the limits of the failure surface can be calculated according to the methodology shown in the Appendix at the end of the paper and Figure 10.

- *Distributed loadings in non-homogenous slopes*: If the projection of a distributed load such as a footing or a pool loading, meets more than one layer on the slip surface, that is, more than one φ' values, then the *distribute*d loadi*ng* should be divided into parts (e.g. see Figure 7b). The resultant force of each one of them should be projected onto an arc of the slip surface having a uniform φ' value along its length.
- *Tension crack*: It is suggested that the tension crack be taken into account as part of the curved surface of a cylinder having axis parallel to the $y-$axis. Moreover, as it is at user's discretion to choose the location of the point of origin of axes, it is more convenient the $z-$coordinate of the center of the slip surface to be chosen equal to zero ($z_C=0$). Thus, the center of the base of the cylinder lies also on the $x-$axis. Moreover, it is assumed that the arc of the cylindrical surface passes through the $(x, z)-$ coordinates of the intersecting points of the sphere, the slope face and the slope crest (points M and N, Figure 11). Therefore in essence, as the curved surface of the cylinder passes through pre-fixed points, the tension crack is defined only by the $x-$coordinate of the base of the cylinder. The computation procedure involves summation and subtraction of volumes.
- *Water in tension crack*: This distribution is triangular as shown in Figure 6, and the resultant force V acts perpendicularly to the tension crack wall at one third of the height of the water. Similar to the case of pool loading, the contact area between water and tension crack must also be known for the calculation of the resultant force V. As the functions representing the contact area of water with the tension crack are known, the area in question derives from the subtraction of the integrals of these two functions; the function of the lower curve represent, in essence, the intersection points between the sphere and the cylinder. The reasonable assumption that V acts at the axis of symmetry of the problem (if it is symmetrical) can be made. As the force V cannot directly be projected onto the failure surface (but gives moment about the center of rotation), it is broken into two components, a radial and a second one, which is perpendicular to the radial component (V_r and V_c, respectively). The first one gives neither moment (as for the center of rotation, O) nor friction force; thus, it can be ignored. The second one is projected onto to the failure surface, where it is broken into tangential and normal component ($V_{c,t}$ and $V_{c,n}$, respectively, see Figure 6). It is noted that the force $V_{c,t}$ produces equal moment as for the point O comparing to the respective one of its mother force, V, that is, $Vy_v = V_c(\text{O}\Pi) = V_{c,t}r$ (see Figure 6). Moreover, as shown in Figure 6, the force V contributes to the friction along the slip surface through the normal component $V_{c,n}$; however, this contribution is rather minor.

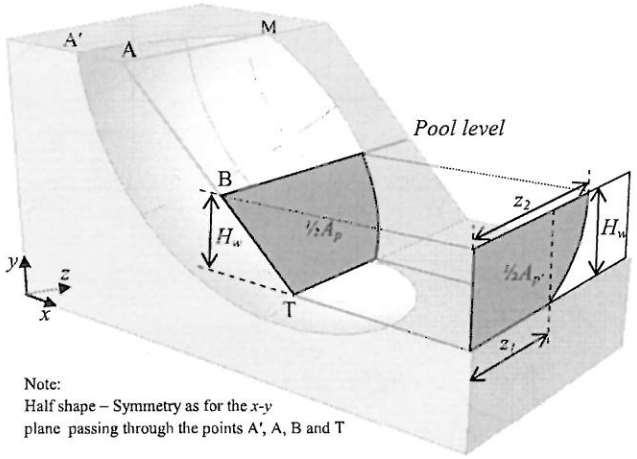

Figure 10. Cylindrical surface considered as the surface of the tension crack.

DOI: 10.1002/nag

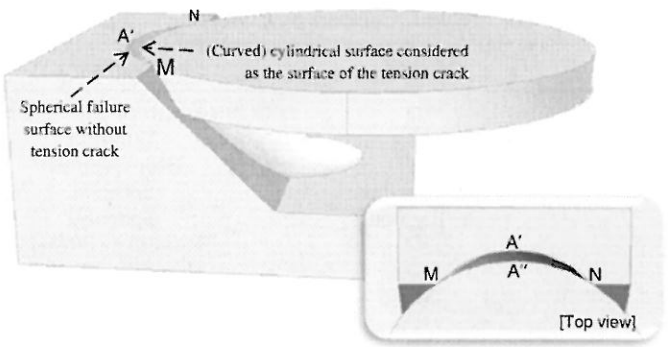

Figure 11. Projection of the contact area between the slope face (inside the limits of the failure surface) and the water because of pool loading on a $z-y$ plane.

7. EXAMPLES

A comparison study is presented relating to the slope shown in Figure 12, which has a dimensionless cohesion strength ratio $c'/\gamma H = 0.116$, friction angle $\varphi' = 15^{\circ}$ and inclination angle 60°. The slope is assumed to have infinite length (in $z-$direction) and is solved by several different methods.

As shown in Table I, the safety factor obtained by the proposed 3D-CFS is comparable to that given by the rigorous version of the method proposed by Huang et al. [1] with a difference of about 1.5%. On the other hand, the simplified version of the method proposed by Huang et al. [1] gives a safety factor value 4.8% lower. Both the rigorous and simplified versions use spherical failure surfaces, and thus, a direct comparison with the proposed 3D-CFS is possible.

Michalowski's charts [6] give safety factor values ranging from 0.996 to 1.340 as a function of the ratio B/H, emphasizing the role of the third dimension on stability. For the same $B/H = 2.55$ ratio, the proposed 3D-CFS method gave $FS = 1.258$ compared with $FS = 1.092$ from Michalowski's charts (15% deviation). A direct comparison with Michalowski cannot be made because that investigator used horn-like failure surfaces as opposed to spherical surfaces by the proposed 3D-CFS. It is accepted, however, that Michalowski's solution is more realistic because it is well known that spherical surfaces, generally, overestimate the factor of safety for frictional soils.

For the same reason as above, a direct comparison between the proposed 3D-CFS and the log-spiral method by Leshchinsky et al. [18] is not possible. It is perhaps surprising though that the method by Leshchinsky et al. [18] gave a higher factor of safety than that delivered by the proposed 3D-CFS using a spherical surface.

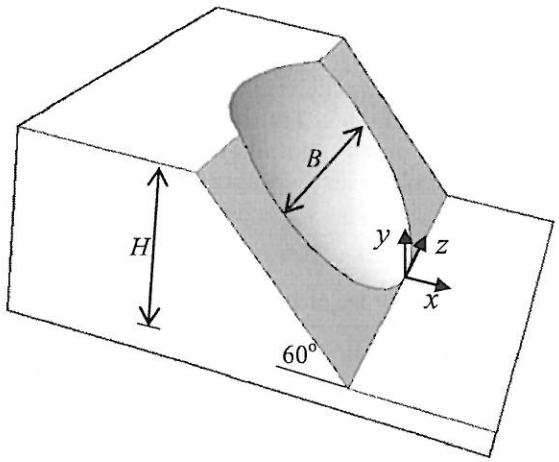

Figure 12. Example: geometry of slope and width of failure.

DOI: 10.1002/nag

Table I. Comparison example.

	Method	Surface	*FS*
Leshchinsky et al. (1985)	3D	Formed by log-spirals	1.25
Hungr et al. (1989)	3D	Ellipsoid	1.23
	(2D)	(Not specified)	(1.00)
Huang et al. (2002)	3D/Simplified	Spherical	1.20
	3D/Rigorous	Spherical	1.24
Michalowski (2010)	3D	Horn-like ($B/H=1$)	1.340
	3D	Horn-like ($B/H=2$)	1.136
	3D	Horn-like ($B/H=2.55$)	1.092
	3D	Horn-like ($B/H=3$)	1.077
	3D	Horn-like ($B/H=5$)	1.040
	(2D)	(Log-spiral)	(0.996)
Proposed CFS	3D	Spherical ($B/H=2.55$)	1.258
	(2D)	(Circular)	(1.004)

Note: B = width of failure calculated by the maximum z –coordinate on the failure surface ($B=2z_{max}$) and H = height of the slope.

Hungr et al. [17] gave $FS=1.23$ for the same slope, but only for a specific failure width-to-length ratio. Because this value does not necessarily correspond to the minimum safety factor for this slope, direct comparison is difficult.

The validity of the assumptions made by any 3D slope stability method, including those proposed by Michalowski, Leshchinsky *et al.* and Hungr *et al.*, can be assessed by comparison with the proposed 3D-CFS. Direct comparison is only possible, however, after applying these assumptions to spherical failure surfaces.

Finally, it is noted that the safety factor of the slope in 2D as given by Hungr *et al.* [17], Michalowski [6] and the proposed 2D-CFS (see Part I for more details about this method) are the same and equal to the unity (Table I).

In addition to the above, two more examples are given in Table II. The two slopes in question have been solved using the proposed 3D-CFS and Michalowski's (2010) charts. As mentioned previously, a direct comparison between the two methods is not possible because of differences in shape of the failure surfaces. However, it can be noted that, although the results are in generally close agreement, the Michalowski results lead to lower values. The horn-like surfaces used by Michalowski were produced by two log-spirals. From 2D analyses, it is known that log-spiral surfaces in frictional soils typically give lower safety factor values compared to the safety factor values obtained by purely circular slip surfaces.

8. CONCLUDING REMARKS

Over the last 40 years, numerous limit equilibrium methods have been proposed for the stability analysis of earth slopes in three dimensions. The majority of them are based on the concept of *columns* as opposed to *slices* used in two-dimensional analyses. The division of a slope into columns, however, renders the problem statically indeterminate, and assumptions are inevitably necessary regarding intercolumn forces. Other methods are based on two-dimensional slope stability

Table II. Examples: Slopes solved by the proposed 3D-CFS and Michalowski's (2010) charts.

# of example	H(m)	β(°)	c' (kPa)	φ' (°)	γ (kN/m^3)	$\frac{B}{H}$	FS_{3d}	$FS_{Mich.}$
1	10	60	20	25.00	20	2.20	1.376	1.251
2	15	75	30	29.05	18	3.44	1.264	1.110

Table note: The safety factor values of the last column ($FS_{Mich.}$) have been obtained by Michalowski's charts (2010) for the same B/H value.

DOI: 10.1002/nag

analyses to estimate three-dimensional stability, whereas more recent approaches to 3D slope stability analysis have included limit analysis and, most recently, finite element methods.

The proposed closed-form solution (CFS) treats the whole sliding mass as a rigid body; thus, the problem becomes statically determinate, and a solution can be found without needing to know the internal state of stress within the failure mass. The CFS method can be applied to non-homogenous slopes with complex geometry together with any kind of external loading. The method is also able to determine the critical location of a tension crack, the shape of which has been assumed to form part of the curved surface of a cylinder. Although it is recognized that the critical failure surface is often non-spherical, the CFS methodology for spheres described herein provides an objective tool for the evaluation of the assumptions made by other limit equilibrium methods including the role of intercolumn forces.

APPENDIX

ANALYTICAL FORMULA FOR THE EXACT CALCULATION OF THE AREA OF THE SLIP SURFACE A_{SS}.

$$A_{ss} = 2\int_0^{z_{\lim}} \{f_1(z) - f_2(z)\}dz \tag{A.1}$$

$$f_1(z) = \left\{ arc\sin\left(\frac{\left| -\sqrt{r^2 - z^2 - (H - y_o)^2} + x_o \right| + x_o}{\sqrt{r^2 - z^2}} \right) - arc\sin\left(\frac{x_o}{r}\right) \right\} r \tag{A.2}$$

$$f_2(z) = \left\{ arc\sin(\omega) - arc\sin\left(\frac{x_o}{r}\right) \right\} r \tag{A.3}$$

where,

$$\omega = \frac{\left| \frac{2(x_o - y_o\tan\beta) + \sqrt{4(x_o - y_o\tan\beta)^2 - 4(1+\tan^2\beta)\left(x_o^2 + y_o^2 + z^2 - r^2\right)}}{2(1+\tan^2\beta)} \right| + x_o}{\sqrt{r^2 - z^2}} \tag{A.4}$$

As mentioned in the text, Eq. (A.1) stands only for symmetrical failures passing through the toe of the slope. Moreover, the point of origin is considered to be the toe of slope for $z = 0$, the upslope area is horizontal ($y = H$), the slope face is represented by a plane parallel to the z −axis and above the negative part of x −axis ($y = -x\tan\beta$); see Figure 1. Thus, for toe failures it stands that $x_o \geq 0$. For other cases it must be modified as needed.

CALCULATION OF THE MAGNITUDE AND POINT OF ACTION OF THE RESULTANT NORMAL AND DRIVING FORCE DUE TO THE WEIGHT OF THE SLIDING MASS

The magnitude and point of action of the resultant normal and driving force due to the weight of the sliding mass are calculated by integrating along the slip surface. First, the sliding mass is divided in the limit as the column widths tend to zero resulting in an infinite number of vertical columns. As the sliding mass is examined as a whole, the intercolumn forces cancel out and therefore, for the sake of brevity, they are ignored. The weight W_{ij} of each column (i^{th} column in the x −direction and j^{th} column in the z −direction; see Figure 13) is broken into two components, one normal $N_{\varphi,ij}$ and one tangential $F_{d,ij}$ to the base (both parallel to the $x-y$plane); integration along the slip surface of these

DOI: 10.1002/nag

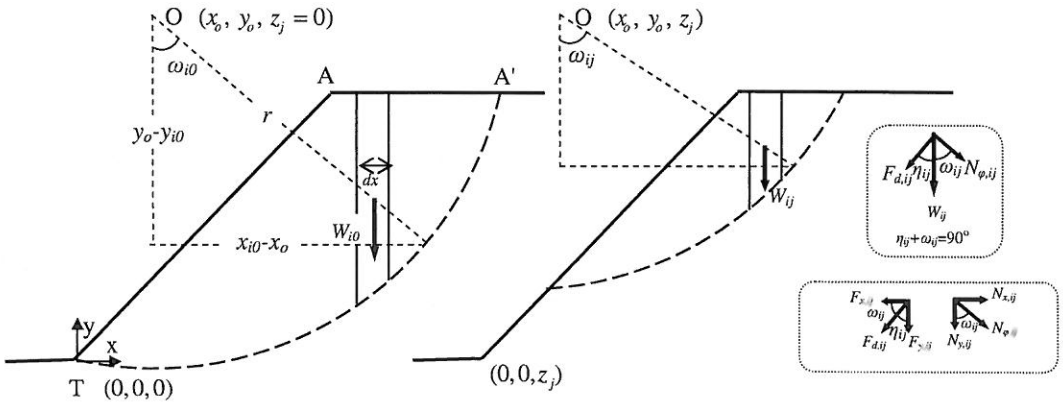

Figure 13. The sliding mass divided into an infinite number of vertical columns.

forces will finally give the resultant normal and driving force respectively (see also the Appendix of Part I [19]). It should be emphasized that the force $N_{\varphi,ij}$ is not the normal reaction at the base of the slice, the magnitude of which is affected by the intercolumn forces. As each one of the $N_{\varphi,ij}$ and $F_{d,ij}$ forces has its own direction, it is necessary that both be analyzed into the $x-$and $y-$directions, that is, $(N_{x,ij}, N_{y,ij})$ and $(F_{x,ij}, F_{y,ij})$ respectively ($N_{z,ij}=0$ and $F_{z,ij}=0$).

Therefore, the magnitude of the three components of the resultant normal force are (Figure 14):

$$N_{R,x} = +\int\int N_{x,ij}dydz = +\int\int N_{ij}\sin\omega_{ij}dydz = \\ = +\int\int W_{ij}(y,z)\sin\omega_{ij}\cos\omega_{ij}dydz \tag{A.5}$$

$$N_{R,y} = -\int\int N_{y,ij}dxdz = -\int\int N_{ij}\cos\omega_{ij}dxdz = \\ = -\int\int W_{ij}(x,z)\cos^2\omega_{ij}dxdz \tag{A.6}$$

$$N_{R,z} = 0 \tag{A.7}$$

Where, ω_{ij} is the angle between the vertical line passing through the point (x_o, y_o, z_j) and the point of action of the weight W_{ij} (center of mass of column $i-j$); see Figure 13.

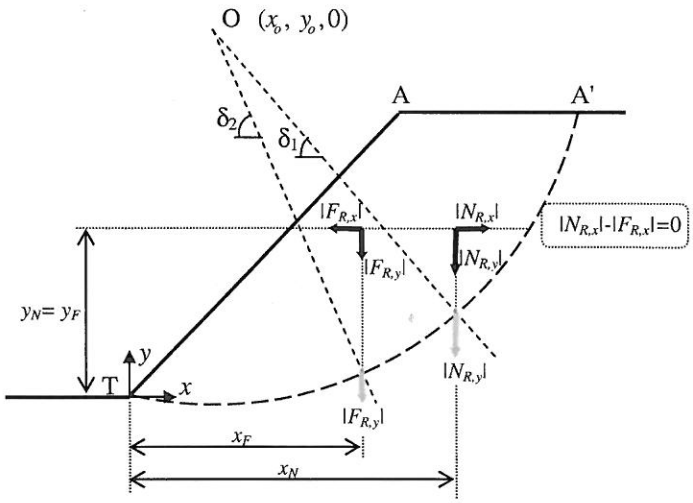

Figure 14. Resultant normal and driving force and their points of action (symmetrical failure).

DOI: 10.1002/nag

Similarly, the magnitude of the three components of the resultant driving force are (Figure 14):

$$F_{R,x} = -\int\int F_{x,ij}dydz = -\int\int F_{d,ij}\cos\omega_{ij}dydz = \\ = -\int\int W_{ij}(y,z)\sin\omega_{ij}\cos\omega_{ij}dydz \tag{A.8}$$

$$F_{R,y} = -\int\int F_{y,ij}dxdz = -\int\int F_{d,ij}\sin\omega_{ij}dxdz \\ = -\int\int W_{ij}(x,z)\sin^2\omega_{ij}dxdz = \\ = -\int\int W_{ij}(x,z)\left(1-\cos^2\omega_{ij}\right)dxdz \tag{A.9}$$

$$F_{R,z} = 0 \tag{A.10}$$

where,

$$\sin\omega_{ij}\cos\omega_{ij} = \frac{x-x_o}{r}\cdot\frac{y_o-y}{r} = \frac{\sqrt{r^2-(y-y_o)^2-z^2}}{r}\cdot\frac{y_o-y}{r} \tag{A.11}$$

$$\cos^2\omega_{ij} = 1-\sin^2\omega_{ij} = 1-\left(\frac{x-x_o}{r}\right)^2 = \\ = 1-\frac{r^2-(y-y_o)^2-z^2}{r^2} = \frac{(y-y_o)^2+z^2}{r^2} \tag{A.12}$$

$$W_{ij}(x,z) = \gamma_s\left\{f_{upper}(x,z)-f_{sph}(x,z)\right\} \tag{A.13}$$

$$W_{ij}(y,z) = \gamma_s\left\{f_{upper}(y,z)-f_{sph}(y,z)\right\} \tag{A.14}$$

The operators in front of the integrals [Eqs. (A.5), (A.6), (A.8) and (A.9)] indicate the direction of force according to a Cartesian coordinate system where the point of origin is the slope toe for $z=0$ and the slope profile is drawn over the positive part of the x −axis. The limits of the integrals in question are defined by the entry and exit point of the slip surface given by the points A′ and T respectively as well as by its lateral limits in third dimension (points M and N); see Figure 1.

The coordinates of the points of action of the resultant normal and driving force are:

$$y_N = \frac{\int\int N_{x,ij}ydydz}{\int\int N_{x,ij}dydz} = \frac{\int\int W_{ij}(y,z)\sin\omega_{ij}\cos\omega_{ij}ydydz}{\int\int W_{ij}(y,z)\sin\omega_{ij}\cos\omega_{ij}dydz} \tag{A.15}$$

$$x_N = \frac{-\int\int N_{y,ij}xdxdz}{-\int\int N_{y,ij}dxdz} = \frac{\int\int W_{ij}(x,z)\cos^2\omega_{ij}xdxdz}{\int\int W_{ij}(x,z)\cos^2\omega_{ij}dxdz} \tag{A.16}$$

$$z_N = 0 \tag{A.17}$$

$$y_F = \frac{-\int F_{x,ij}ydydz}{-\int\int F_{x,ij}dydz} = \frac{\int\int W_{ij}(y,z)\sin\omega_{ij}\cos\omega_{ij}ydydz}{\int\int W_{ij}(y,z)\sin\omega_{ij}\cos\omega_{ij}dydz} \tag{A.18}$$

$$x_F = \frac{-\int\int F_{y,ij}xdxdz}{-\int\int F_{y,ij}dxdz} = \frac{\int\int W_{ij}(x,z)\left(1-\cos^2\omega_{ij}\right)xdxdz}{\int\int W_{ij}(x,z)\left(1-\cos^2\omega_{ij}\right)dxdz} \tag{A.19}$$

$$z_F = 0 \tag{A.20}$$

DOI: 10.1002/nag

It may be noted that as all components of the normal and driving forces given by Eqs. (A.5)-(A.10) are generated by the gravitational weight of the sliding mass which is obviously vertical, the following equations must be satisfied:

$$N_{R,x} + F_{R,x} = 0 \tag{A.21}$$

$$N_{R,y} + F_{R,y} = W \tag{A.22}$$

$$N_{R,z} + F_{R,z} = 0 \tag{A.23}$$

Substituting Eqs. (A.5)-(A.10) into Eqs. (A.21), (A.22) and (A.23) it can easily be shown that both preconditions are true. Moreover, from Eqs. (A.15) and (A.18) it is observed that the points of action of the resultant normal and driving force have the same $y-$coordinate, that is, $y_N = y_F$.

Finally, from the above and taking into account the buoyancy force U, the safety factor expression of Eq. (A.24) is obtained. For the cohesion and buoyancy force as well as for any possible external loading it stands what it has been written in the main text. Eq. (A.24) is the rigorous expression of safety factor which gives exactly the same result with the simplified one [Eq. (3)].

$$FS_M = \frac{rc'A_{ss} + r\left(|N_{R,y}|\sin\delta_1 + |F_{R,y}|\sin\delta_2\right)\tan\varphi' - rU\tan\varphi'}{r\left(|N_{R,y}|\cos\delta_1 + |F_{R,y}|\cos\delta_2\right)} \tag{A.24}$$

CALCULATION OF THE AREA A_P

- Let the function of the slope face, which is assumed parallel to the $z-$axis, be $y = f_{sf}(x)$ or expressed as for y, $x = f_{sf}(y)$.
- Substituting $x = f_{sf}(y)$ in the equation of sphere $f_{sph}(x, y, z)$, the points of intersection between the sphere and the slope face are given by Eq. (A.25). In essence, the total of these points along with the lines $y = 0$ and $y = H_w$ form an area, which is the projection of the area A_p on a $y - z$ plane (Fig. 10).

$$\left(f_{sf}(y) - x_o\right)^2 + (y - y_o)^2 + z^2 = r^2 \rightarrow y = f(z) \tag{A.25}$$

- The projection of the area A_p on the plane $y - z$ has area equal to:

$$A_{p'} = 2\left(z_1 H_w + \int_{z_1}^{z_2} (H_w - |f(z)|)dz\right) \tag{A.25}$$

where, z_1 and z_2 are the integration limits, which can be found by substituting $y = 0$ and $y = H_w$ respectively into Eq. (A.25) and solving as for z; $z_1 = 0$ for toe failures.

- Finally, the inclined area A_p is equal to:

$$A_p = {}^{A_{p'}}/_{\sin\beta} \tag{A.27}$$

ACKNOWLEDGEMENTS

The authors wish to acknowledge the support of the following: (i) NSF grant CMMI-0970122 on 'GOALI: Probabilistic Geomechanical Analysis in the Exploitation of Unconventional Resources'; (ii) KGHM Cuprum, Wrocław, Poland through the Framework 7 EU project on 'Industrial Risk Reduction' (IRIS).

DOI: 10.1002/nag

NOTATION

A_p	Contact area between the water (pool loading) and the slope face inside the limits of the failure surface in m^2
$A_{p'}$	Projection of area A_p in a $z-y$ plane in m^2
A_{ss}	Area of the slip surface in m^2
B	Width of failure (in z −direction) measured on the slope face in m
c'	Cohesion with respect to effective stresses in kN/m^2
E_v and E_h	Vertical and horizontal component of seismic force respectively in kN
F_c	Force due to cohesion (resultant) in kN
F_φ	Friction force (resultant) in kN
F_u	Friction force caused by the pore pressure force $U(F_u = U\tan\varphi')$ in kN
F_f	Footing force (concentrated loading) in kN
$f_i(x)$ or $f_i(y)$	Mathematical functions representing the geometric elements of the problem (e.g. slope face, upslope area)
$f_{sf}(x)$ or $f_{sf}(y)$	Mathematical functions representing the slope face (see Appendix)
$f_{sph}(x, y, z)$	Equation of sphere $(x-x_o)^2+(y-y_o)^2+z^2=r^2$
FS_M	Safety factor with respect of moments used in definition
FS_{3d}	Safety factor with respect of moments referring to three dimensions
$FS_{3d,F}$	Safety factor with respect of forces referring to three dimensions
$g_i(x)$	Mathematical function representing the interface between two successive soil layers
H	Slope height in meters
H_w	Pool height in meters
$h_{w,i}$	Height water measured vertically from the slip surface in a given position i in meters
M_f and M_d	Sum of the resisting and driving moments respectively in kNm
r	The radius of the slip surface in meters, which is considered spherical
$\tan\beta$	Slope gradient
$u(x, y, z)$	Function representing the pore pressure distribution along the slip surface
U	Pore pressure force (resultant; $U=\Sigma u$) in kN
V	The resultant force due to water in tension crack in kN
V_r and V_c	The radial and perpendicular to the radial component of force V in kN
V_p	The resultant force due to pool surcharge acting on the failure surface in kN
W	Weight of the sliding mass in kN
x_o and y_o	The x and y −coordinate, respectively, of the center of the slip sphere in meters ($z_o=0$).
x_C, y_C and z_C	The x, y and z − coordinate, respectively, of the center of the failure mass in meters
$x_{C'}$ and $y_{C'}$	The x and $y$coordinate, respectively, of the center of mass of the area bounded between the slip surface and the free water surface in meters
γ_s and γ_w	Specific gravity of soil and water, respectively, in kN/m^3
σ	Total normal stress in kN/m^2
τ	Effective shear strength in kN/m^2
φ'	Friction angle of soil material with respect to effective shear stresses in degrees
Subscripts n and t	Subscripts under force notation indicate normal and tangential component, respectively

REFERENCES

1. Huang C, Tsai C, Chen Y. Generalized method for three-dimensional slope stability analysis. *Journal of Geotechnical and Geoenvironmental Engineering* 2002; **128**(10):836–848.
2. Michalowski RL. Three dimensional analysis of locally loaded slopes. *Geotechnique* 1989; **39**(1):27–38.
3. Hungr O. An extension of Bishop's simplified method of slope stability analysis to three dimensions. *Geotechnique* 1987; **37**(1):113–117.
4. Hovland HJ. Three-dimensional slope stability analysis method. *Journal of the Geotechnical Engineering Division* 1977; **103**(9):971–986.

DOI: 10.1002/nag

5. Loehr JE, McCoy BF, Wright G. Quasi-three-dimensional slope stability analysis method for general sliding bodies. *Journal of Geotechnical and Geoenvironmental Engineering* 2004; **130**(6):551–560.
6. Michalowski RL. Limit analysis and stability charts for 3D slope failures. *Journal of Geotechnical and Geoenvironmental Engineering* 2010; **136**(4):583–593.
7. Yu HS, Salgado R, Sloan SW, Kim JM. Limit analysis versus limit equilibrium for slope stability. *Journal of Geotechnical and Geoenvironmental Engineering* 1998; **124**(1):1–11.
8. Farzaneh O, Askari F. Three-dimensional analysis of nonhomogeneous slopes. *Journal of Geotechnical and Geoenvironmental Engineering* 2003; **129**(2):137–145.
9. Chen Z, Wang J, Wang Y, Yin JH, Haberfield C. A three-dimensional slope stability analysis method using the upper bound theorem. Part I: numerical approaches, applications and extensions. *International Journal of Rock Mechanics and Mining Sciences* 2001b; **38**(3):379–397.
10. Chen Z, Wang X, Haberfield C, Yin JH, Wang Y. A three-dimensional slope stability analysis method using the upper bound theorem. Part I: theory and methods. *International Journal of Rock Mechanics and Mining Sciences* 2001a; **38**(3):369–378.
11. Griffiths DV, Marquez RM. Three-dimensional slope stability analysis by elasto-plastic finite elements. *Geotechnique* 2007; **57**(6):537–546.
12. Griffiths DV, Marquez RM. Discussion: Three-dimensional slope stability analysis by elasto-plastic finite elements. *Geotechnique* 2008; **58**(8):683–685.
13. Sainak AN. Application of three-dimensional finite element method in parametric and geometric studies of slope stability. In *Advances in geotechnical engineering: The Skempton conference*, Jardine RJ, Potts DM, Higgins KG (eds.) Vol. **2**. Thomas Telford: London, 2004; 933–942.
14. Cheng YM, Lau CK. *Slope stability analysis and stabilization: New methods and insight*. Taylor & Francis: New York, 2008.
15. Duncan JM, Wright SG. *Soil strength and slope stability*. John Wiley and Sons: New York, 2005.
16. Duncan JM. State of the art: limit equilibrium and finite-element analysis of slopes. *Journal of Geotechnical Engineering* 1996; **122**(7):577–596.
17. Hungr O, Salgado FM, Byrne PM. Evaluation of a three-dimensional method of slope stability analysis. *Canadian Geotechnical Journal* 1989; **26**:679–686.
18. Leshchinsky D, Baker R, Silver ML. Three-dimensional analysis of slope stability. *International Journal for Numerical and Analytical Methods in Geomechanics* 1985; **9**:199–223.
19. Panteliids L, Griffiths DV, Silver ML. Stability of earth slopes. Part I: 2D analysis in closed-form. *International Journal for Numerical and Analytical Methods in Geomechanics* 2012; Published ahead of print

DOI: 10.1002/nag